

Vertical stress distribution in isotropic half-spaces due to surface vertical loadings acting over polygonal domains

Maria Grazia D'Urso^{1,*} and F. Marmo²

¹ DICeM – Department of Civil and Mechanical Engineering, University of Cassino and of Lazio Meridionale, via G. Di Biasio 43, 03043 Cassino (Fr), Italy

² Department of Structures in Engineering and Architecture, University of Naples Federico II, Naples, Italy

Received 12 February 2013, revised 6 June 2013, accepted 22 August 2013

Published online ♣ 2013

Key words Stress analysis, foundations, potential theory, finite elements.

By integrating the classical Boussinesq expression we derive analytically the vertical stress distribution induced by pressures distributed with arbitrary laws, up to the third order, over polygonal domains. Thus, one can evaluate in closed form either the vertical stress produced by shell elements, modelling raft foundations by finite elements, acting over a Winkler soil or those induced by a linear pressure distribution simulating axial force and biaxial bending moments over a pad foundation. To this end we include charts and tables, both for rectangular and circular domains, which allow the designer to evaluate the vertical stresses induced by linear load distributions by hand calculations. The effectiveness of the proposed approach is witnessed by the comparison between the analytical results obtained with the proposed formulas and the numerical ones of a FEM discretization of the soil associated with the loading distribution induced by a foundation modeled by plate elements resting on a Winkler soil.

© 2013 WILEY-VCH Verlag GmbH & Co. KGaA, Weinheim

1 Introduction

The classical approach to finding stress and displacements in an elastic, homogeneous and isotropic half-space due to surface tractions has been first developed by Boussinesq [4] who provided the solution for a point load by making use of the potential theory [3].

The case of uniform pressure applied within a circular domain was addressed by Lamb [19] while Love [20] considered the case of isotropic uniform pressure applied within a rectangular region.

However, even in many natural soils deposited through a geologic process of sedimentation over a period of time stiffness becomes greater with depth. Analytical continuum models reflecting this property were first studied by Gibson [16] by assuming incompressibility and a linear increase of soil stiffness with depth. In later papers Gibson further refined his model and presented on account of his results in a Rankine lecture [17].

Subsequently Vrettos [30] solved the Boussinesq problem for an half-space exhibiting an exponential behavior of stiffness yet with a bounded value at infinite depth. Half-spaces of this kind were later studied by Selvadurai in the framework of contact static problems and a survey account of his result were presented in [24].

Since the pioneering work by Gibson an abundant literature has been published on the evaluation of stresses and displacements in inhomogeneous and/or anisotropic half-spaces, see e.g. [31] for a fairly complete account.

Nevertheless, Boussinesq solution is still widely used mainly for its elegance and conciseness, for instance to evaluate the order of magnitude of the depth of influence of a foundation load [7] and the related settlement. Actually, it is usually assumed that the variation of vertical stress with depth below a loaded region on the surface can be predicted with sufficient accuracy using linear, homogeneous, isotropic elastic theory.

Further applications of this theory range, to quote only a few, from space geodesy to contact mechanics, rock mechanics and geomechanics.

For instance, in the former case position-time series recorded by continuous GPS stations exhibit seasonal fluctuations due to surface loading associated with changes in atmospheric and sea-floor pressure, shifting masses of snow/ice and surface water [8, 21]. Usually, problems with localized loads do have a spatial scale which is very small when compared with Earth's radius so that the problem can be assimilated to that of a half-space.

* Corresponding author E-mail: durso@unicas.it

In contact mechanics [18] classical Hertz theory assumes that for the purpose of calculating the local deformations of two bodies in contact each body can be regarded as an elastic half-space loaded over a small elliptical region of its plane surface.

In rock mechanics [31] the magnitude and distribution of the displacements and stresses in rocks are predicted by using solutions that model rock as a linearly elastic, homogeneous and isotropic continuum. Only for rock masses cut by discontinuities, these solutions should account for anisotropy.

Clearly the most significant field of application of the results contributed by Boussinesq is in geomechanics in order to predict stress values in soil masses [6] induced by foundation loads.

Actually the Boussinesq solutions have been integrated for a large number of load cases of particular interest in applications. For example the closed form solution of vertical stress at a depth below the corner of a uniformly loaded rectangular region was derived by Newmark [22], a solution further improved by Stainbrenner and presented in form of simple design charts [6].

Vitone and Valsangkar [29] evaluated the vertical stress induced by a linearly distributed loading while the vertical stress under the corner of a linearly loaded triangular domain was obtained in [25]. Some of the analytical results were later collected by Poulos and Davis [23].

More recently the closed-form solution of vertical stress distribution associated with a linearly distributed surface pressure over rectangles was presented by Algin [1, 2] and extended in [10] by addressing surface loadings linearly distributed over polygonal regions of arbitrary shape.

In this paper we consider the case of surface pressure distributions represented by third-order polynomials in both coordinates of a 2D reference frame assumed on the surface of the half-space. This is motivated by the kind of loads which can be applied on a Winkler soil by shell elements currently employed in finite element softwares for modeling raft foundations. Actually the shape functions considered in shell elements for vertical, i.e. out of plane, displacements are usually represented by third-order polynomials, as a maximum, so that proportionality of pressures to displacement dictated by Winkler model yields a third-order pressure distribution.

The vertical stress at an arbitrary point within the half-space is obtained analytically by means of formulas expressed solely as a function of the coordinates of the vertices of the loaded region, assumed to be of arbitrary polygonal shape. The result is obtained by transforming to line integrals the 2D integrals coming out from the application of the superposition principles to the loading region.

Analogously to up-to-date application of potential theory in geodesy [11–14], this has been possible by suitable variants of Gauss theorem, some of which are proved for convenience. The same rationale has been exploited to solve the companion problem of evaluating the displacements within the half-space induced by surface loads [15].

To illustrate the practical application of the proposed formulas to the evaluation of the vertical stresses induced in the soil by a foundation analyzed by the finite element method we consider a numerical example regarding a wall footing modeled by means of plate elements on Winkler soil. The analytical results obtained by the proposed approach are successfully compared with the numerical ones obtained by applying the same load pattern to a finite element model of the soil.

Finally some design aids are included in form of charts and tables, both for rectangular and circular foundations, in order to allow the designer to perform hand calculations of vertical stress produced by linearly distributed surface pressures.

2 Definition of the problem

Let (O, x, y, z) be an orthonormal reference system and Π be a homogeneous and isotropic half-space having the plane $z = 0$ as boundary; we further assume that the z axis is directed downwards.

According to the classical solution first contributed by Boussinesq [4], a point load F_z , directed vertically and acting at the origin of the reference frame induces a vertical stress at a generic point $\mathbf{p} = (x, y, z)^t$ in the half-space defined by:

$$\sigma_z(\mathbf{p}) = -\frac{3F_z}{2\pi} \frac{z^3}{(\mathbf{p} \cdot \mathbf{p})^{\frac{5}{2}}} = -\frac{3F_z}{2\pi} \frac{z^3}{(x^2 + y^2 + z^2)^{\frac{5}{2}}}. \quad (1)$$

Being interested to the evaluation of the vertical stress induced by rather arbitrary distributions of vertical loads it is more convenient to assume a new reference frame in which the origin is given by the intersection of the plane $z = 0$, i.e. the boundary of the half-space, with the vertical along the point at which the stress is going to be evaluated, see e.g. Fig. 1. Actually, by the reciprocity theorem [28] we can write:

$$\sigma_z(0, 0, z) = -\frac{3F_z}{2\pi} \frac{z^3}{(\boldsymbol{\rho} \cdot \boldsymbol{\rho} + z^2)^{\frac{5}{2}}} \quad (2)$$

where we have introduced the vector $\boldsymbol{\rho} = (x, y)^t$ collecting the coordinates of the applied load.

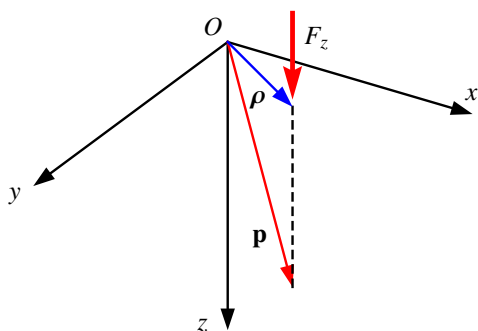


Fig. 1 Reference frame.

Objective of this paper is to further generalize the results previously contributed in [10] by evaluating analytically the vertical stress induced by a load distribution defined by the expression:

$$q(\rho) = q_0 + \mathbf{g} \cdot \boldsymbol{\rho} + \mathbf{A} \cdot (\boldsymbol{\rho} \otimes \boldsymbol{\rho}) + \mathbb{B} \cdot (\boldsymbol{\rho} \otimes \boldsymbol{\rho} \otimes \boldsymbol{\rho}) \quad (3)$$

where q_0 , \mathbf{g} , \mathbf{A} , and \mathbb{B} are in turn scalar, vector, second-order and third-order tensors. The second order tensor $\boldsymbol{\rho} \otimes \boldsymbol{\rho}$ has a matrix representation of the kind:

$$[\boldsymbol{\rho} \otimes \boldsymbol{\rho}] = \begin{bmatrix} x^2 & xy \\ xy & y^2 \end{bmatrix} \quad (4)$$

so that, being:

$$\mathbf{A} \cdot (\boldsymbol{\rho} \otimes \boldsymbol{\rho}) = A_{11}x^2 + 2A_{12}xy + A_{22}y^2 \quad (5)$$

a quadratic distribution of loads can be assigned on the half space by suitably defining the coefficients of the symmetric tensor \mathbf{A} .

Analogously, we introduce the third-order tensors \mathbb{B} and $\boldsymbol{\rho} \otimes \boldsymbol{\rho} \otimes \boldsymbol{\rho}$, represented in matrix form as:

$$\mathbb{B} = \begin{bmatrix} \mathbb{B}_{111} & \mathbb{B}_{112} \\ \mathbb{B}_{121} & \mathbb{B}_{122} \\ \mathbb{B}_{211} & \mathbb{B}_{212} \\ \mathbb{B}_{221} & \mathbb{B}_{222} \end{bmatrix}, \quad \boldsymbol{\rho} \otimes \boldsymbol{\rho} \otimes \boldsymbol{\rho} = \begin{bmatrix} x \begin{bmatrix} x^2 & xy \\ xy & y^2 \end{bmatrix} \\ y \begin{bmatrix} x^2 & xy \\ xy & y^2 \end{bmatrix} \end{bmatrix} \quad (6)$$

i.e. as vectors of rank-two tensors; they can be used to assign a cubic distribution of loads in the form:

$$\mathbb{B} \cdot (\boldsymbol{\rho} \otimes \boldsymbol{\rho} \otimes \boldsymbol{\rho}) = \mathbb{B}_{111}x^3 + (\mathbb{B}_{112} + \mathbb{B}_{121} + \mathbb{B}_{211})x^2y + (\mathbb{B}_{122} + \mathbb{B}_{212} + \mathbb{B}_{221})xy^2 + \mathbb{B}_{222}y^3 \quad (7)$$

by assuming:

$$\mathbb{B}_{112} = \mathbb{B}_{121} = \mathbb{B}_{211}, \quad \mathbb{B}_{122} = \mathbb{B}_{212} = \mathbb{B}_{221} \quad (8)$$

for symmetry of representation.

The apparently unusual load distribution (3) is motivated by the loads induced on a half-space, modelled as a Winkler soil, by a raft foundation analyzed by means of shell elements. Actually the shape functions for the transversal displacements are usually represented, as a maximum, by third-order polynomials so that assuming a constant Winkler coefficient for the soil, the load distribution produced by each element can be represented by formula (3).

Therefore, according to (2), the vertical stress σ_q induced at the origin of the reference frame by a load distribution of the kind (3) is given by:

$$\begin{aligned} \sigma_q &= -\frac{3z^3}{2\pi} \left[q_0 \int_{\Omega} \frac{d\Omega}{(\boldsymbol{\rho} \cdot \boldsymbol{\rho} + z^2)^{\frac{5}{2}}} + \mathbf{g} \cdot \int_{\Omega} \frac{\boldsymbol{\rho} d\Omega}{(\boldsymbol{\rho} \cdot \boldsymbol{\rho} + z^2)^{\frac{5}{2}}} + \mathbf{A} \cdot \int_{\Omega} \frac{(\boldsymbol{\rho} \otimes \boldsymbol{\rho}) d\Omega}{(\boldsymbol{\rho} \cdot \boldsymbol{\rho} + z^2)^{\frac{5}{2}}} \right. \\ &\quad \left. + \mathbb{B} \cdot \int_{\Omega} \frac{(\boldsymbol{\rho} \otimes \boldsymbol{\rho} \otimes \boldsymbol{\rho}) d\Omega}{(\boldsymbol{\rho} \cdot \boldsymbol{\rho} + z^2)^{\frac{5}{2}}} \right] \\ &= -\frac{3z^3}{2\pi} [q_0 I_0 + \mathbf{g} \cdot \mathbf{i}_1 + \mathbf{A} \cdot \mathbf{I}_2 + \mathbb{B} \cdot \mathbf{I}_3] \end{aligned} \quad (9)$$

where Ω is the domain on which the load distribution (3) is applied.

We are going to prove that whenever Ω is polygonal the stress σ_q can be computed analytically by evaluating the integrals I_0 , \mathbf{i}_1 , \mathbf{I}_2 , and \mathbf{I}_3 in closed form. To this end we shall assume $z \neq 0$ since, otherwise, equilibrium dictates trivially $\sigma_q = 0$ if the origin of the reference frame does not belong to Ω and $\sigma_q = -q(\mathbf{0})$ in the opposite case.

In order to evaluate the integrals (9) we shall suitably extend the general approach, based on the application of the Gauss theorem, first contributed in [10, 12].

3 Evaluation of I_0

The first integral in (9) can be evaluated by considering the integral:

$$\int_{\Omega} \operatorname{div} \left[\frac{\boldsymbol{\rho}}{(\boldsymbol{\rho} \cdot \boldsymbol{\rho})(\boldsymbol{\rho} \cdot \boldsymbol{\rho} + z^2)^{\frac{3}{2}}} \right] d\Omega \quad (10)$$

where 'div' stands for the divergence operator.

Notice that the integrand becomes singular if $\boldsymbol{\rho} = \mathbf{0}$, i.e. if the origin of the reference frame does belong to the loading area Ω . We shall prove, however, that basic results of distribution theory, [27], and of differential calculus, [5], can be suitably invoked to derive a well-defined formula for the computation of the integral I_0 appearing in (9).

Invoking the differential identity [27]:

$$\operatorname{div}(\phi \mathbf{u}) = \operatorname{grad} \phi \cdot \mathbf{u} + \phi \operatorname{div} \mathbf{u} \quad (11)$$

where 'grad' denotes the gradient operator and ϕ / \mathbf{u} a continuous scalar / vector field, one has:

$$\begin{aligned} \int_{\Omega} \operatorname{div} \left[\frac{\boldsymbol{\rho}}{(\boldsymbol{\rho} \cdot \boldsymbol{\rho})(\boldsymbol{\rho} \cdot \boldsymbol{\rho} + z^2)^{\frac{3}{2}}} \right] d\Omega &= \int_{\Omega} \frac{\boldsymbol{\rho}}{\boldsymbol{\rho} \cdot \boldsymbol{\rho}} \cdot \operatorname{grad} \left[\frac{1}{(\boldsymbol{\rho} \cdot \boldsymbol{\rho} + z^2)^{\frac{3}{2}}} \right] d\Omega \\ &+ \int_{\Omega} \frac{1}{(\boldsymbol{\rho} \cdot \boldsymbol{\rho} + z^2)^{\frac{3}{2}}} \operatorname{div} \frac{\boldsymbol{\rho}}{\boldsymbol{\rho} \cdot \boldsymbol{\rho}} d\Omega. \end{aligned} \quad (12)$$

Being:

$$\operatorname{grad} \frac{1}{(\boldsymbol{\rho} \cdot \boldsymbol{\rho} + z^2)^{\frac{3}{2}}} = -3 \frac{\boldsymbol{\rho}}{(\boldsymbol{\rho} \cdot \boldsymbol{\rho} + z^2)^{\frac{5}{2}}} \quad (13)$$

the first integral on the right-hand side becomes:

$$\int_{\Omega} \frac{\boldsymbol{\rho}}{\boldsymbol{\rho} \cdot \boldsymbol{\rho}} \cdot \operatorname{grad} \left[\frac{1}{(\boldsymbol{\rho} \cdot \boldsymbol{\rho} + z^2)^{\frac{3}{2}}} \right] d\Omega = -3 \int_{\Omega} \frac{1}{(\boldsymbol{\rho} \cdot \boldsymbol{\rho} + z^2)^{\frac{5}{2}}} d\Omega. \quad (14)$$

The singularity for $\boldsymbol{\rho} = 0$ in the argument of the divergence operator in (12) can be accounted for by invoking distribution theory [27] and the differential identity (11) to get:

$$\operatorname{div} \frac{\boldsymbol{\rho}}{\boldsymbol{\rho} \cdot \boldsymbol{\rho}} = 0 \quad \text{if } \boldsymbol{\rho} \neq \mathbf{0} \quad (15)$$

while [10]:

$$\int_{\Omega} \phi(\boldsymbol{\rho}) \operatorname{div} \left[\frac{\boldsymbol{\rho}}{\boldsymbol{\rho} \cdot \boldsymbol{\rho}} \right] = \begin{cases} 0 & \text{if } \mathbf{0} \notin \Omega \\ \alpha(\mathbf{0})\phi(\mathbf{0}) & \text{if } \mathbf{0} \in \Omega \end{cases} \quad (16)$$

where α represents the angular measure, expressed in radians, of the intersection between Ω and a circular neighborhood of the singularity point $\boldsymbol{\rho} = \mathbf{0}$. Hence:

$$\alpha(\mathbf{0}) = \begin{cases} 2\pi & \text{if } \mathbf{0} \in \overset{\circ}{\Omega} \\ \pi & \text{if } \mathbf{0} \in \overline{\partial\Omega} \\ f(\pi) & \text{if } \mathbf{0} \in \partial\Omega \setminus \overline{\partial\Omega} \end{cases} \quad (17)$$

where $\overset{\circ}{\Omega}$ denotes the interior of Ω and $\overline{\partial\Omega}$ the set of the regular points of the boundary $\partial\Omega$, i.e. the points at which the tangent is defined. Should Ω be polygonal and the origin coincide with a vertex of Ω , $\alpha(\mathbf{0})$ simply measures the angle formed by the two consecutive sides of $\partial\Omega$ intersecting at the origin. A general algorithm for computing $\alpha(\mathbf{0})$ can be found in [9].

To sum up:

$$\int_{\Omega} \frac{1}{(\boldsymbol{\rho} \cdot \boldsymbol{\rho} + z^2)^{\frac{5}{2}}} \operatorname{div} \frac{\boldsymbol{\rho}}{\boldsymbol{\rho} \cdot \boldsymbol{\rho}} d\Omega = \frac{\alpha(\mathbf{0})}{z^3} \quad (18)$$

which is always well defined for $z \neq 0$.

In conclusion, formula (14) and the previous equation yield:

$$\int_{\Omega} \operatorname{div} \left[\frac{\boldsymbol{\rho}}{(\boldsymbol{\rho} \cdot \boldsymbol{\rho})(\boldsymbol{\rho} \cdot \boldsymbol{\rho} + z^2)^{\frac{3}{2}}} \right] d\Omega = \frac{\alpha(\mathbf{0})}{z^3} - 3 \int_{\Omega} \frac{1}{(\boldsymbol{\rho} \cdot \boldsymbol{\rho} + z^2)^{\frac{5}{2}}} d\Omega \quad (19)$$

so that, applying the divergence theorem to the integral on the left-hand side of the previous equation one finally has:

$$I_0 = \int_{\Omega} \frac{d\Omega}{(\boldsymbol{\rho} \cdot \boldsymbol{\rho} + z^2)^{\frac{5}{2}}} = \frac{\alpha(\mathbf{0})}{3z^3} - \frac{1}{3} \int_{\partial\Omega} \frac{\boldsymbol{\rho} \cdot \boldsymbol{\nu}}{(\boldsymbol{\rho} \cdot \boldsymbol{\rho})(\boldsymbol{\rho} \cdot \boldsymbol{\rho} + z^2)^{\frac{3}{2}}} d\Omega. \quad (20)$$

We shall now proceed to evaluate analytically the previous integral for a polygonal domain.

3.1 Closed form evaluation of I_0 for a polygonal domain

Let us suppose that the boundary $\partial\Omega$ of the loading area is a polygon defined by n_v vertices whose position is defined in the given reference frame by vectors $\boldsymbol{\rho}_i = (x_i, y_i)$, $i = 1, \dots, n_v$.

The integral I_0 can thus be written as:

$$I_0 = \frac{\alpha(\mathbf{0})}{3z^3} - \frac{1}{3} \sum_{i=1}^{n_v} \int_0^{l_i} \frac{\boldsymbol{\rho}(s_i) \cdot \boldsymbol{\nu}_i}{[\boldsymbol{\rho}(s_i) \cdot \boldsymbol{\rho}(s_i)][\boldsymbol{\rho}(s_i) \cdot \boldsymbol{\rho}(s_i) + z^2]^{\frac{3}{2}}} ds_i \quad (21)$$

where s_i is the curvilinear abscissa along the i -th edge of the polygon, measured from the vertex i , $l_i = |\boldsymbol{\rho}_{i+1} - \boldsymbol{\rho}_i|$ is the length of the i -th edge, defined by means of the initial ($\boldsymbol{\rho}_i$) and the end vertex ($\boldsymbol{\rho}_{i+1}$), and $\boldsymbol{\nu}_i$ is the outward unit vector to the i -th edge of $\partial\Omega$. This last one can be evaluated as:

$$\boldsymbol{\nu}_i = \frac{\boldsymbol{\rho}_{i+1}^\perp - \boldsymbol{\rho}_i^\perp}{l_i} \quad (22)$$

where $(\cdot)^\perp$ stands for a vector orthogonal to (\cdot) . In particular, assuming a counter-clockwise circulation sense along the boundary of Ω , $(\cdot)^\perp$ denotes a clockwise rotation of the vector (\cdot) ; hence, making reference to $\boldsymbol{\rho}_i = (x_i, y_i)$ to fix the ideas, $\boldsymbol{\rho}_i^\perp = (y_i, -x_i)$.

To evaluate the integral (21) we introduce the parameter representation of the i -th edge of $\partial\Omega$ in the form:

$$\boldsymbol{\rho}[\lambda_i(s_i)] = [1 - \lambda_i(s_i)]\boldsymbol{\rho}_i + \lambda_i(s_i)\boldsymbol{\rho}_{i+1} \quad \lambda_i(s_i) \in [0, 1] \quad (23)$$

where $\lambda_i(s_i) = s_i/l_i$.

Accordingly, the expression of I_0 in (21) becomes:

$$I_0 = \frac{\alpha(\mathbf{0})}{3z^3} - \frac{1}{3} \sum_{i=1}^{n_v} (\boldsymbol{\rho}_i \cdot \boldsymbol{\rho}_{i+1}^\perp) H_{0i} \quad (24)$$

where:

$$H_{0i} = \int_0^1 \frac{1}{(a_i \lambda_i^2 + 2 b_i \lambda_i + c_i)(a_i \lambda_i^2 + 2 b_i \lambda_i + d_i)^{\frac{3}{2}}} d\lambda_i \quad (25)$$

and:

$$\begin{aligned} a_i &= (\boldsymbol{\rho}_{i+1} - \boldsymbol{\rho}_i) \cdot (\boldsymbol{\rho}_{i+1} - \boldsymbol{\rho}_i); & b_i &= \boldsymbol{\rho}_i \cdot (\boldsymbol{\rho}_{i+1} - \boldsymbol{\rho}_i); \\ c_i &= \boldsymbol{\rho}_i \cdot \boldsymbol{\rho}_i; & d_i &= \boldsymbol{\rho}_i \cdot \boldsymbol{\rho}_i + z^2. \end{aligned} \quad (26)$$

Provided that $\rho_i \neq \rho_{i+1}$, i.e. no vertex of the polygon is counted twice, it turns out to be $a_i > 0$; furthermore $c_i \geq 0$ and $d_i > 0$ since it has been assumed $z \neq 0$.

Performing the change of variable:

$$t_i = \lambda_i + \frac{b_i}{a_i} \quad (27)$$

and setting:

$$\begin{aligned} t_{i0} &= \frac{b_i}{a_i}; & t_{i1} &= 1 + \frac{b_i}{a_i}; \\ A_i &= \frac{c_i}{a_i} - \frac{b_i^2}{a_i^2}; & B_i &= \frac{d_i}{a_i} - \frac{b_i^2}{a_i^2} \end{aligned} \quad (28)$$

the integral (25) becomes:

$$H_{0i} = \frac{1}{a_i^{\frac{5}{2}}} \int_{t_{i0}}^{t_{i1}} \frac{1}{(A_i + t_i^2)(B_i + t_i^2)^{\frac{3}{2}}} dt_i \quad (29)$$

which yields:

$$\begin{aligned} H_{0i} &= \frac{1}{a_i^{\frac{5}{2}}} \left[\frac{t_i}{B_i(A_i - B_i) \sqrt{B_i + t_i^2}} + \frac{\arctan \left[\frac{t_i \sqrt{B_i - A_i}}{\sqrt{A_i(B_i + t_i^2)}} \right]}{\sqrt{A_i(B_i - A_i)}^{\frac{3}{2}}} \right]_{t_{i0}}^{t_{i1}} \\ &= \frac{1}{a_i^{\frac{5}{2}}} \left\{ \frac{t_{i1}}{B_i(A_i - B_i) \sqrt{B_i + t_{i1}^2}} - \frac{t_{i0}}{B_i(A_i - B_i) \sqrt{B_i + t_{i0}^2}} \right. \\ &\quad \left. + \frac{\arctan \left[\frac{t_{i1} \sqrt{B_i - A_i}}{\sqrt{A_i(B_i + t_{i1}^2)}} \right] - \arctan \left[\frac{t_{i0} \sqrt{B_i - A_i}}{\sqrt{A_i(B_i + t_{i0}^2)}} \right]}{\sqrt{A_i(B_i - A_i)}^{\frac{3}{2}}} \right\} \end{aligned} \quad (30)$$

The square roots $\sqrt{B_i + t_{i1}^2}$ and $\sqrt{B_i + t_{i0}^2}$ are always well defined since (26) and (28) imply that $B_i > A_i \geq 0$, the last inequality following from Cauchy-Schwarz inequality [27]. However A_i may become zero if the origin of the reference frame coincides with a vertex or belongs to an edge of the boundary $\partial\Omega$.

In the former case, the condition $\rho_i = \mathbf{0}$ would imply $b_i = c_i = 0$ in (26), $A_i = 0$ in (28) and an undefined value for H_{0i} . However, in this case H_{0i} needs not to be computed since $\rho_i = \mathbf{0}$ in (24).

If $\mathbf{0}$ does not coincide with a vertex of $\partial\Omega$ but belongs to one of its edges $A_i = 0$ as well. This condition can be equivalently stated as $\rho_i \cdot \rho_{i+1}^\perp = 0$ so that the relevant addend in (24) is zero and the computation of H_{0i} irrelevant.

In conclusion formula (24) must be corrected as follows:

$$I_0 = \frac{\alpha(\mathbf{0})}{3z^3} - \frac{1}{3} \sum_{i=1, i \neq j}^{n_p} (\rho_i \cdot \rho_{i+1}^\perp) H_{0i} \quad \text{if } \rho_i = \mathbf{0} \text{ or } \rho_i \cdot \rho_{i+1}^\perp = 0. \quad (31)$$

Invoking (28) the integral H_{0i} can be written as :

$$\begin{aligned} H_{0i} &= \frac{b_i}{z^2(a_i d_i - b_i^2) \sqrt{d_i}} - \frac{a_i + b_i}{z^2(a_i d_i - b_i^2) \sqrt{a_i + 2b_i + d_i}} \\ &\quad + \frac{a}{z^3 \sqrt{a_i c_i - b_i^2}} \left[\arctan \frac{z(a_i + b_i)}{\sqrt{a_i c_i - b_i^2} \sqrt{a_i + 2b_i + d_i}} - \arctan \frac{z b_i}{\sqrt{a_i c_i - b_i^2} \sqrt{d_i}} \right] \end{aligned} \quad (32)$$

which is well defined since it is easy to verify that:

$$a_i + 2b_i + d_i = \rho_{i+1} \cdot \rho_{i+1} + z^2 > 0 \quad (33)$$

while the condition:

$$a_i c_i - b_i^2 > 0 \quad (34)$$

holds true since it is equivalent to the previously stated condition $B_i > A_i$.

4 Evaluation of \mathbf{i}_1

Let us now illustrate the analytical evaluation of the second integral in (9). It is straightforward to verify that:

$$\mathbf{i}_1 = \int_{\Omega} \frac{\rho d\Omega}{(\rho \cdot \rho + z^2)^{\frac{5}{2}}} = -\frac{1}{3} \int_{\Omega} \text{grad} \left[\frac{1}{(\rho \cdot \rho + z^2)^{\frac{3}{2}}} \right] d\Omega \quad (35)$$

where 'grad' stands for the gradient operator.

Invoking for the last integral a special form of the divergence theorem [5] one gets:

$$\mathbf{i}_1 = -\frac{1}{3} \int_{\partial\Omega} \frac{\nu ds}{(\rho \cdot \rho + z^2)^{\frac{3}{2}}}. \quad (36)$$

Remark 1. Although well-known in classical textbooks of tensor analysis it is instructive to provide a simple proof of the previous result since it represents the rationale to derive less standard results exploited in the sequel.

Considering the rank-two identity tensor \mathbf{I} , a scalar field $\phi(\rho)$ and adopting the indicial notation the divergence of the composition of \mathbf{I} and ϕ is given by:

$$\text{div}(\mathbf{I}\phi) = [I_{ij}\phi]_{,j} = \delta_{ij}\phi_{,j} = \phi_{,i} = \text{grad}\phi \quad (37)$$

Hence, integrating over Ω and applying the divergence theorem:

$$\int_{\Omega} \text{grad}\phi d\Omega = \int_{\Omega} \text{div}(\mathbf{I}\phi) d\Omega = \int_{\partial\Omega} \mathbf{I}\phi \nu ds = \int_{\partial\Omega} \phi \nu ds \quad (38)$$

which is the identity used to derive (36).

4.1 Closed form evaluation of \mathbf{i}_1 for a polygonal domain

In the case of a polygonal domain the integral (36) can be expressed as sum of n_v line integrals by applying the same path of reasoning illustrated in Sect. 3.1. Thus,

$$\mathbf{i}_1 = -\frac{1}{3} \sum_{i=1}^{n_v} \int_0^{l_i} \frac{\nu_i}{[\rho_i(s_i) \cdot \rho_i(s_i) + z^2]^{\frac{3}{2}}} ds_i \quad (39)$$

or, equivalently,

$$\mathbf{i}_1 = -\frac{1}{3} \sum_{i=1}^{n_v} (\rho_{i+1}^{\perp} - \rho_i^{\perp}) \int_0^1 \frac{1}{(a_i \lambda_i^2 + 2b_i \lambda_i + d_i)^{\frac{3}{2}}} d\lambda_i = -\frac{1}{3} \sum_{i=1}^{n_v} (\rho_{i+1}^{\perp} - \rho_i^{\perp}) H_{1i} \quad (40)$$

where a_i , b_i , and d_i have been defined in (26). The integral H_{1i} is given by:

$$\begin{aligned} H_{1i} &= \int_0^1 \frac{1}{(a_i \lambda_i^2 + 2b_i \lambda_i + d_i)^{\frac{3}{2}}} d\lambda_i = - \left[\frac{b_i + a_i \lambda_i}{(b_i^2 - a_i d_i) \sqrt{a_i \lambda_i^2 + 2b_i \lambda_i + d_i}} \right]_0^1 \\ &= \frac{1}{b_i^2 - a_i d_i} \left(\frac{b_i}{\sqrt{d_i}} - \frac{a_i + b_i}{\sqrt{a_i + 2b_i + d_i}} \right) \end{aligned} \quad (41)$$

and is well defined due to (26) and (33).

5 Evaluation of \mathbf{I}_2

Let us now turn our attention to the third integral in (9):

$$\mathbf{I}_2 = \int_{\Omega} \frac{\boldsymbol{\rho} \otimes \boldsymbol{\rho}}{(\boldsymbol{\rho} \cdot \boldsymbol{\rho} + z^2)^{\frac{3}{2}}} d\Omega. \quad (42)$$

To this end we first recall the differential identity [5]:

$$\text{grad}(\phi \mathbf{u}) = \mathbf{u} \otimes \text{grad} \phi + \phi \text{grad} \mathbf{u} \quad (43)$$

where ϕ and \mathbf{u} are in turn scalar and vector fields; we thus infer:

$$\text{grad} \left[\frac{\boldsymbol{\rho}}{(\boldsymbol{\rho} \cdot \boldsymbol{\rho} + z^2)^{\frac{3}{2}}} \right] = -3 \frac{\boldsymbol{\rho} \otimes \boldsymbol{\rho}}{(\boldsymbol{\rho} \cdot \boldsymbol{\rho} + z^2)^{\frac{5}{2}}} + \frac{\mathbf{I}}{(\boldsymbol{\rho} \cdot \boldsymbol{\rho} + z^2)^{\frac{3}{2}}}. \quad (44)$$

Hence:

$$\begin{aligned} \mathbf{I}_2 &= -\frac{1}{3} \int_{\Omega} \text{grad} \left[\frac{\boldsymbol{\rho}}{(\boldsymbol{\rho} \cdot \boldsymbol{\rho} + z^2)^{\frac{3}{2}}} \right] d\Omega + \frac{\mathbf{I}}{3} \int_{\Omega} \frac{d\Omega}{(\boldsymbol{\rho} \cdot \boldsymbol{\rho} + z^2)^{\frac{3}{2}}} \\ &= -\frac{1}{3} \int_{\partial\Omega} \frac{\boldsymbol{\rho} \otimes \boldsymbol{\nu}}{(\boldsymbol{\rho} \cdot \boldsymbol{\rho} + z^2)^{\frac{3}{2}}} d\Omega + \frac{\mathbf{I}}{3} \int_{\Omega} \frac{d\Omega}{(\boldsymbol{\rho} \cdot \boldsymbol{\rho} + z^2)^{\frac{3}{2}}} \end{aligned} \quad (45)$$

Remark 2. Following the same path of reasoning illustrated in Remark 1 the previous identity can be obtained by applying the divergence theorem to the composition of the rank-four tensor \mathbb{I} whose indicial notation is given by $[\mathbb{I}]_{ijkl} = \delta_{il} \delta_{jk}$ and a vector field \mathbf{u} . Actually, one has:

$$\text{div}(\mathbb{I} \mathbf{u}) = \delta_{il} \delta_{jk} u_{l,k} = u_{i,j} = \text{grad} \mathbf{u} \quad (46)$$

so that the integration over Ω of the previous identity yields the desired result.

To compute the last integral above we invoke (11) to get:

$$\text{div} \left[\frac{\boldsymbol{\rho}}{(\boldsymbol{\rho} \cdot \boldsymbol{\rho} + z^2)^{\frac{1}{2}}} \right] = -\frac{\boldsymbol{\rho} \cdot \boldsymbol{\rho}}{(\boldsymbol{\rho} \cdot \boldsymbol{\rho} + z^2)^{\frac{3}{2}}} + \frac{2}{(\boldsymbol{\rho} \cdot \boldsymbol{\rho} + z^2)^{\frac{1}{2}}} \quad (47)$$

or, equivalently, adding and subtracting z^2 to the numerator of the first addend on the right-hand side:

$$\text{div} \left[\frac{\boldsymbol{\rho}}{(\boldsymbol{\rho} \cdot \boldsymbol{\rho} + z^2)^{\frac{1}{2}}} \right] = \frac{z^2}{(\boldsymbol{\rho} \cdot \boldsymbol{\rho} + z^2)^{\frac{3}{2}}} + \frac{1}{(\boldsymbol{\rho} \cdot \boldsymbol{\rho} + z^2)^{\frac{1}{2}}}. \quad (48)$$

Hence, by the Gauss theorem:

$$\int_{\Omega} \frac{d\Omega}{(\boldsymbol{\rho} \cdot \boldsymbol{\rho} + z^2)^{\frac{3}{2}}} = \frac{1}{z^2} \int_{\partial\Omega} \frac{\boldsymbol{\rho} \cdot \boldsymbol{\nu}}{(\boldsymbol{\rho} \cdot \boldsymbol{\rho} + z^2)^{\frac{1}{2}}} ds - \frac{1}{z^2} \int_{\Omega} \frac{d\Omega}{(\boldsymbol{\rho} \cdot \boldsymbol{\rho} + z^2)^{\frac{1}{2}}}. \quad (49)$$

The last integral above has been calculated in formula (18) of [12] and is provided by:

$$\int_{\Omega} \frac{d\Omega}{(\boldsymbol{\rho} \cdot \boldsymbol{\rho} + z^2)^{\frac{1}{2}}} = \int_{\partial\Omega} \frac{(\boldsymbol{\rho} \cdot \boldsymbol{\rho} + z^2)^{\frac{1}{2}} (\boldsymbol{\rho} \cdot \boldsymbol{\nu})}{\boldsymbol{\rho} \cdot \boldsymbol{\rho}} ds - z\alpha(\mathbf{0}). \quad (50)$$

In conclusion, combining formulas (45), (49), and (50) one finally gets:

$$\begin{aligned} \mathbf{I}_2 &= \int_{\Omega} \frac{\boldsymbol{\rho} \otimes \boldsymbol{\rho}}{(\boldsymbol{\rho} \cdot \boldsymbol{\rho} + z^2)^{\frac{3}{2}}} = -\frac{1}{3} \int_{\partial\Omega} \frac{\boldsymbol{\rho} \otimes \boldsymbol{\nu} ds}{(\boldsymbol{\rho} \cdot \boldsymbol{\rho} + z^2)^{\frac{3}{2}}} + \frac{\mathbf{I}}{3z^2} \int_{\partial\Omega} \frac{\boldsymbol{\rho} \cdot \boldsymbol{\nu}}{(\boldsymbol{\rho} \cdot \boldsymbol{\rho} + z^2)^{\frac{1}{2}}} \\ &\quad - \frac{\mathbf{I}}{3z^2} \int_{\partial\Omega} \frac{(\boldsymbol{\rho} \cdot \boldsymbol{\rho} + z^2)^{\frac{1}{2}} (\boldsymbol{\rho} \cdot \boldsymbol{\nu})}{\boldsymbol{\rho} \cdot \boldsymbol{\rho}} ds + \frac{\mathbf{I}}{3z} \alpha(\mathbf{0}) \\ &= -\frac{1}{3} \mathbf{A}_2 + \frac{\mathbf{I}}{3z^2} (B_2 - C_2) + \frac{\mathbf{I}}{3z} \alpha(\mathbf{0}) \end{aligned} \quad (51)$$

i.e. an expression which allows one to compute \mathbf{I}_2 solely by means of integrals extended to $\partial\Omega$.

5.1 Closed form evaluation of \mathbf{I}_2 for a polygonal domain

Assuming Ω to be polygonal, formula (51) is the starting point to express \mathbf{I}_2 as linear combination of rank-two quantities depending solely upon the coordinates of the vertices of $\partial\Omega$.

To this end let us proceed to compute separately the tensor \mathbf{A}_2 and the scalars B_2 and C_2 appearing in (51). One has:

$$\mathbf{A}_2 = \int_{\partial\Omega} \frac{\boldsymbol{\rho} \otimes \boldsymbol{\nu} ds}{(\boldsymbol{\rho} \cdot \boldsymbol{\rho} + z^2)^{\frac{3}{2}}} = \sum_{i=1}^{n_v} \left\{ \int_0^{l_i} \frac{\boldsymbol{\rho}(s_i)}{[\boldsymbol{\rho}(s_i) \cdot \boldsymbol{\rho}(s_i) + z^2]^{\frac{3}{2}}} ds_i \right\} \otimes \boldsymbol{\nu}_i \quad (52)$$

or equivalently, by means of (23):

$$\begin{aligned} \mathbf{A}_2 &= \sum_{i=1}^{n_v} \left[\boldsymbol{\rho}_i \otimes (\boldsymbol{\rho}_{i+1}^\perp - \boldsymbol{\rho}_i^\perp) \int_0^1 \frac{d\lambda_i}{(a_i \lambda_i^2 + 2b_i \lambda_i + d_i)^{\frac{3}{2}}} \right. \\ &\quad \left. + (\boldsymbol{\rho}_{i+1} - \boldsymbol{\rho}_i) \otimes (\boldsymbol{\rho}_{i+1}^\perp - \boldsymbol{\rho}_i^\perp) \int_0^1 \frac{\lambda_i d\lambda_i}{(a_i \lambda_i^2 + 2b_i \lambda_i + d_i)^{\frac{3}{2}}} \right] \\ &= \sum_{i=1}^{n_v} \left[\boldsymbol{\rho}_i \otimes (\boldsymbol{\rho}_{i+1}^\perp - \boldsymbol{\rho}_i^\perp) H_{1i}^{A_2} + (\boldsymbol{\rho}_{i+1} - \boldsymbol{\rho}_i) \otimes (\boldsymbol{\rho}_{i+1}^\perp - \boldsymbol{\rho}_i^\perp) H_{2i}^{A_2} \right]. \end{aligned} \quad (53)$$

It turns out to be:

$$H_{1i}^{A_2} = \frac{1}{b_i^2 - a_i d_i} \left(\frac{b_i}{\sqrt{d_i}} - \frac{a_i + b_i}{\sqrt{a_i + 2b_i + d_i}} \right) \quad (54)$$

and:

$$H_{2i}^{A_2} = \frac{1}{b_i^2 - a_i d_i} \left(\frac{b_i + d_i}{\sqrt{a_i + 2b_i + d_i}} - \sqrt{d_i} \right) \quad (55)$$

where a_i , b_i , and d_i are defined in (26). Both the previous integrals are well defined due to (33).

Furthermore:

$$\begin{aligned} B_2 &= \int_{\partial\Omega} \frac{\boldsymbol{\rho} \cdot \boldsymbol{\nu}}{(\boldsymbol{\rho} \cdot \boldsymbol{\rho} + z^2)^{\frac{1}{2}}} = \sum_{i=1}^{n_v} \int_0^{l_i} \frac{\boldsymbol{\rho}(s_i) \cdot \boldsymbol{\nu}_i}{[\boldsymbol{\rho}(s_i) \cdot \boldsymbol{\rho}(s_i) + z^2]^{\frac{1}{2}}} ds_i \\ &= \sum_{i=1}^{n_v} (\boldsymbol{\rho}_i \cdot \boldsymbol{\rho}_{i+1}^\perp) \int_0^1 \frac{d\lambda_i}{(a_i \lambda_i^2 + 2b_i \lambda_i + d_i)^{\frac{1}{2}}} = \sum_{i=1}^{n_v} (\boldsymbol{\rho}_i \cdot \boldsymbol{\rho}_{i+1}^\perp) H_i^{B_2} \end{aligned} \quad (56)$$

where:

$$H_i^{B_2} = \frac{1}{\sqrt{a_i}} \ln \frac{a_i + b_i + \sqrt{a_i(a_i + 2b_i + d_i)}}{b_i + \sqrt{a_i d_i}}. \quad (57)$$

As repeatedly specified above a_i and d_i are positive as well as $a_i + 2b_i + d_i$.

Finally:

$$\begin{aligned} C_2 &= \int_{\partial\Omega} \frac{(\boldsymbol{\rho} \cdot \boldsymbol{\rho} + z^2)^{\frac{1}{2}} (\boldsymbol{\rho} \cdot \boldsymbol{\nu}) ds}{\boldsymbol{\rho} \cdot \boldsymbol{\rho}} = \sum_{i=1}^{n_v} \int_0^{l_i} \frac{[\boldsymbol{\rho}(s_i) \cdot \boldsymbol{\rho}(s_i) + z^2]^{\frac{1}{2}} [\boldsymbol{\rho}(s_i) \cdot \boldsymbol{\nu}_i] ds_i}{\boldsymbol{\rho}(s_i) \cdot \boldsymbol{\rho}(s_i)} \\ &= \sum_{i=1}^{n_v} (\boldsymbol{\rho}_i \cdot \boldsymbol{\rho}_{i+1}^\perp) \int_0^1 \frac{(a_i \lambda_i^2 + 2b_i \lambda_i + d_i)^{\frac{1}{2}} d\lambda_i}{(a_i \lambda_i^2 + 2b_i \lambda_i + c_i)} = \sum_{i=1}^{n_v} (\boldsymbol{\rho}_i \cdot \boldsymbol{\rho}_{i+1}^\perp) H_i^{C_2}. \end{aligned} \quad (58)$$

Adopting the change of variable (27) and the definitions (28) one has:

$$H_i^{C_2} = \frac{1}{\sqrt{a_i}} \left\{ \frac{\sqrt{B_i - A_i}}{\sqrt{A_i}} \left[\arctan \frac{t_{i1} \sqrt{B_i - A_i}}{\sqrt{A_i(B_i + t_{i1}^2)}} - \arctan \frac{t_{i0} \sqrt{B_i - A_i}}{\sqrt{A_i(B_i + t_{i0}^2)}} \right] + \ln \frac{t_{i1} + \sqrt{B_i + t_{i1}^2}}{t_{i0} + \sqrt{B_i + t_{i0}^2}} \right\} \quad (59)$$

or, equivalently:

$$H_i^{C_2} = \frac{z}{\sqrt{a_i c_i - b_i^2}} \left[\arctan \frac{z(a_i + b_i)}{\sqrt{a_i c_i - b_i^2} \sqrt{a_i + 2b_i + d_i}} - \arctan \frac{z b_i}{\sqrt{a_i c_i - b_i^2} \sqrt{d_i}} \right] + \frac{1}{\sqrt{a_i}} \ln \frac{a_i + b_i + \sqrt{a_i(a_i + 2b_i + d_i)}}{b_i + \sqrt{a_i d_i}}. \quad (60)$$

Notice that the addends in the square parentheses do coincide with the analogous terms in (32) contributing to the expression of H_{0i} while the last term coincides with $H_i^{B_2}$ in (57).

6 Evaluation of \mathbb{I}_3

The evaluation of the vertical stresses σ_q provided by (9) requires finally the evaluation of the integral \mathbb{I}_3 defined by:

$$\mathbb{I}_3 = \int_{\Omega} \frac{\boldsymbol{\rho} \otimes \boldsymbol{\rho} \otimes \boldsymbol{\rho}}{(\boldsymbol{\rho} \cdot \boldsymbol{\rho} + z^2)^{\frac{5}{2}}} d\Omega. \quad (61)$$

It can be evaluated by invoking the differential identity:

$$\text{grad}(\phi \mathbf{A}) = \mathbf{A} \otimes \text{grad} \phi + \phi \text{grad} \mathbf{A} \quad (62)$$

which generalizes the identity (43) to the case of third-order tensors.

In particular:

$$\text{grad} \frac{\boldsymbol{\rho} \otimes \boldsymbol{\rho}}{(\boldsymbol{\rho} \cdot \boldsymbol{\rho} + z^2)^{\frac{3}{2}}} = -3 \frac{\boldsymbol{\rho} \otimes \boldsymbol{\rho} \otimes \boldsymbol{\rho}}{(\boldsymbol{\rho} \cdot \boldsymbol{\rho} + z^2)^{\frac{5}{2}}} + \frac{\text{grad}(\boldsymbol{\rho} \otimes \boldsymbol{\rho})}{(\boldsymbol{\rho} \cdot \boldsymbol{\rho} + z^2)^{\frac{3}{2}}} \quad (63)$$

where:

$$\text{grad}(\boldsymbol{\rho} \otimes \boldsymbol{\rho}) = \hat{\mathbf{I}} \otimes \boldsymbol{\rho} + \boldsymbol{\rho} \otimes \mathbf{I} \quad (64)$$

and $\hat{\mathbf{I}} \otimes \boldsymbol{\rho}$ is the third order tensor expressed in indicial notation as:

$$(\hat{\mathbf{I}} \otimes \boldsymbol{\rho})_{ijk} = I_{ik} \rho_j. \quad (65)$$

Hence, formulas (63) and (64) yield:

$$\int_{\Omega} \frac{\boldsymbol{\rho} \otimes \boldsymbol{\rho} \otimes \boldsymbol{\rho}}{(\boldsymbol{\rho} \cdot \boldsymbol{\rho} + z^2)^{\frac{5}{2}}} d\Omega = \frac{1}{3} \left[\int_{\Omega} \frac{\boldsymbol{\rho} d\Omega}{(\boldsymbol{\rho} \cdot \boldsymbol{\rho} + z^2)^{\frac{3}{2}}} \otimes \mathbf{I} + \hat{\mathbf{I}} \otimes \int_{\Omega} \frac{\boldsymbol{\rho} d\Omega}{(\boldsymbol{\rho} \cdot \boldsymbol{\rho} + z^2)^{\frac{3}{2}}} - \int_{\partial\Omega} \frac{\boldsymbol{\rho} \otimes \boldsymbol{\rho} \otimes \boldsymbol{\nu}}{(\boldsymbol{\rho} \cdot \boldsymbol{\rho} + z^2)^{\frac{3}{2}}} ds \right] \quad (66)$$

where the Gauss theorem has been applied to the left-hand side of (63).

Remark 3. The previous unusual form of the Gauss theorem stems from the following considerations. Let us consider the sixth-order identity tensor \mathbb{I}^6 expressed in indicial notation as $[\mathbb{I}^6]_{ijklmn} = \delta_{in} \delta_{jm} \delta_{kl}$ and an arbitrary tensor field $\mathbf{T}(\boldsymbol{\rho})$. Evaluating the divergence of the composition $\mathbb{I}^6 \mathbf{T}$:

$$\text{div}[\mathbb{I}^6 \mathbf{T}] = \delta_{in} \delta_{jm} \delta_{kl} T_{nm,l} = T_{ij,k} = \text{grad} \mathbf{T} \quad (67)$$

and integrating over Ω yields the result exploited in (66) upon the application of the divergence theorem.

To compute the first and second integrals on the right-hand side of (66) we observe that:

$$\int_{\Omega} \frac{\boldsymbol{\rho} d\Omega}{(\boldsymbol{\rho} \cdot \boldsymbol{\rho} + z^2)^{\frac{3}{2}}} = - \int_{\Omega} \text{grad} \frac{1}{(\boldsymbol{\rho} \cdot \boldsymbol{\rho} + z^2)^{\frac{1}{2}}} d\Omega = - \int_{\partial\Omega} \frac{\boldsymbol{\nu} ds}{(\boldsymbol{\rho} \cdot \boldsymbol{\rho} + z^2)^{\frac{1}{2}}}. \quad (68)$$

To sum up it turns out to be:

$$\mathbb{I}_3 = -\frac{1}{3} \left[\int_{\partial\Omega} \frac{\boldsymbol{\nu} ds}{(\boldsymbol{\rho} \cdot \boldsymbol{\rho} + z^2)^{\frac{1}{2}}} \otimes \mathbf{I} + \hat{\mathbf{I}} \otimes \int_{\partial\Omega} \frac{\boldsymbol{\nu} ds}{(\boldsymbol{\rho} \cdot \boldsymbol{\rho} + z^2)^{\frac{1}{2}}} + \int_{\partial\Omega} \frac{\boldsymbol{\rho} \otimes \boldsymbol{\rho} \otimes \boldsymbol{\nu}}{(\boldsymbol{\rho} \cdot \boldsymbol{\rho} + z^2)^{\frac{3}{2}}} ds \right] \quad (69)$$

so that \mathbb{I}_3 is expressed solely by means of boundary integrals.

6.1 Closed form evaluation of \mathbb{I}_3 for a polygonal domain

For a polygonal domain Ω formula (69) specializes as follows. The first two integrals on the right-hand side of (69) become:

$$\begin{aligned} \mathbf{a}_3 &= \int_{\partial\Omega} \frac{\boldsymbol{\nu} ds}{(\boldsymbol{\rho} \cdot \boldsymbol{\rho} + z^2)^{\frac{1}{2}}} = \sum_{i=1}^{n_v} \boldsymbol{\nu}_i \int_0^{l_i} \frac{ds_i}{[\boldsymbol{\rho}(s_i) \cdot \boldsymbol{\rho}(s_i) + z^2]^{\frac{1}{2}}} \\ &= \sum_{i=1}^{n_v} (\boldsymbol{\rho}_{i+1}^\perp - \boldsymbol{\rho}_i^\perp) \int_0^1 \frac{d\lambda_i}{(a_i \lambda_i^2 + 2b_i \lambda_i + d_i)^{\frac{1}{2}}}. \end{aligned} \quad (70)$$

Being:

$$H_i^{a_3} = \int_0^1 \frac{d\lambda_i}{(a_i \lambda_i^2 + 2b_i \lambda_i + d_i)^{\frac{1}{2}}} = \frac{1}{\sqrt{a_i}} \ln \frac{a_i + b_i + \sqrt{a_i(a_i + 2b_i + d_i)}}{b_i + \sqrt{a_i d_i}} \quad (71)$$

it turns out to be:

$$\mathbf{a}_3 = (\boldsymbol{\rho}_{i+1}^\perp - \boldsymbol{\rho}_i^\perp) H_i^{a_3}. \quad (72)$$

Furthermore, invoking (23):

$$\begin{aligned} \mathbb{B}_3 &= \int_{\partial\Omega} \frac{\boldsymbol{\rho} \otimes \boldsymbol{\rho} \otimes \boldsymbol{\nu}}{(\boldsymbol{\rho} \cdot \boldsymbol{\rho} + z^2)^{\frac{3}{2}}} ds = \sum_{i=1}^{n_v} \left[\int_0^{l_i} \frac{\boldsymbol{\rho}(s_i) \otimes \boldsymbol{\rho}(s_i)}{[\boldsymbol{\rho}(s_i) \cdot \boldsymbol{\rho}(s_i) + z^2]^{\frac{3}{2}}} ds_i \right] \otimes \boldsymbol{\nu}_i \\ &= \sum_{i=1}^{n_v} \left\{ \boldsymbol{\rho}_i \otimes \boldsymbol{\rho}_i \int_0^1 \frac{d\lambda_i}{(a_i \lambda_i^2 + 2b_i \lambda_i + d_i)^{\frac{3}{2}}} \right. \\ &\quad + [\boldsymbol{\rho}_i \otimes (\boldsymbol{\rho}_{i+1} - \boldsymbol{\rho}_i) + (\boldsymbol{\rho}_{i+1} - \boldsymbol{\rho}_i) \otimes \boldsymbol{\rho}_i] \int_0^1 \frac{\lambda_i d\lambda_i}{(a_i \lambda_i^2 + 2b_i \lambda_i + d_i)^{\frac{3}{2}}} \\ &\quad \left. + (\boldsymbol{\rho}_{i+1} - \boldsymbol{\rho}_i) \otimes (\boldsymbol{\rho}_{i+1} - \boldsymbol{\rho}_i) \int_0^1 \frac{\lambda_i^2 d\lambda_i}{(a_i \lambda_i^2 + 2b_i \lambda_i + d_i)^{\frac{3}{2}}} \right\} \otimes (\boldsymbol{\rho}_{i+1}^\perp - \boldsymbol{\rho}_i^\perp). \end{aligned} \quad (73)$$

The first two integrals above have been already computed in (54):

$$H_{1i}^{B_3} = H_{1i}^{A_2} = \int_0^1 \frac{d\lambda_i}{(a_i \lambda_i^2 + 2b_i \lambda_i + d_i)^{\frac{3}{2}}} = \frac{1}{b_i^2 - a_i d_i} \left(\frac{b_i}{\sqrt{d_i}} - \frac{a_i + b_i}{\sqrt{a_i + 2b_i + d_i}} \right) \quad (74)$$

and (55):

$$H_{2i}^{B_3} = H_{2i}^{A_2} = \int_0^1 \frac{\lambda_i d\lambda_i}{(a_i \lambda_i^2 + 2b_i \lambda_i + d_i)^{\frac{3}{2}}} = \frac{1}{b_i^2 - a_i d_i} \left(\frac{b_i + d_i}{\sqrt{a_i + 2b_i + d_i}} - \sqrt{d_i} \right). \quad (75)$$

The last integral in (73) is given by:

$$\begin{aligned} H_{3i}^{B_3} &= \int_0^1 \frac{\lambda_i^2 d\lambda_i}{(a_i \lambda_i^2 + 2b_i \lambda_i + d_i)^{\frac{3}{2}}} \\ &= \frac{2b_i^2 - a_i d_i + b_i d_i - b_i \sqrt{d_i(a_i + 2b_i + d_i)}}{a_i(a_i d_i - b_i^2) \sqrt{a_i + 2b_i + d_i}} + \frac{1}{a_i^{\frac{3}{2}}} \ln \frac{a_i + b_i + \sqrt{a_i(a_i + 2b_i + d_i)}}{b_i + \sqrt{a_i d_i}} \end{aligned} \quad (76)$$

so that we get finally:

$$\begin{aligned} \mathbb{I}_3 &= -\frac{1}{3} \left\{ \left[\sum_{i=1}^{n_v} H_i^{a_3} (\boldsymbol{\rho}_{i+1}^\perp - \boldsymbol{\rho}_i^\perp) \right] \otimes \mathbf{I} + \hat{\mathbf{I}} \otimes \left[\sum_{i=1}^{n_v} H_i^{a_3} (\boldsymbol{\rho}_{i+1}^\perp - \boldsymbol{\rho}_i^\perp) \right] \right. \\ &\quad + \sum_{i=1}^{n_v} \left\{ (\boldsymbol{\rho}_i \otimes \boldsymbol{\rho}_i) H_{1i}^{B_3} + [\boldsymbol{\rho}_i \otimes (\boldsymbol{\rho}_{i+1} - \boldsymbol{\rho}_i) + (\boldsymbol{\rho}_{i+1} - \boldsymbol{\rho}_i) \otimes \boldsymbol{\rho}_i] H_{2i}^{B_3} \right. \\ &\quad \left. \left. + (\boldsymbol{\rho}_{i+1} - \boldsymbol{\rho}_i) \otimes (\boldsymbol{\rho}_{i+1} - \boldsymbol{\rho}_i) H_{3i}^{B_3} \right\} \otimes (\boldsymbol{\rho}_{i+1}^\perp - \boldsymbol{\rho}_i^\perp) \right\}. \end{aligned} \quad (77)$$

7 Numerical examples

We illustrate hereafter some applications of the general approach outlined in the previous sections in order to solve practical problems in foundation engineering.

In particular, the formulas derived thus far are intended mainly as a programming tool for evaluating the vertical stress induced by vertical loads distributed with the law (3) over polygonal domains. Nevertheless such formulas have been applied for plotting charts which can be used for evaluating the vertical stress induced by simple load cases by hand calculations; in particular, we shall make reference to the cases of a rectangular or a circular loaded region by adopting the superposition principle. Such data can also be used to solve more complex loading cases as illustrated in the sequel.

As last example we consider a more complex case represented by the foundation of a wall with an arbitrary geometry. Aim of the example is to evaluate the vertical stress induced in the soil by the foundation and comparing the values predicted by the analytical formulas contributed in the paper with the numerical ones obtained by a FEM discretization of the soil.

7.1 Rectangular domain subject to a linear pressure distribution

Let us evaluate the vertical stress at depth z under the corner of a rectangle of size $D_L \times D_B$ loaded with a uniform pressure distribution, as shown in Fig. 2(a), or a linear pressure distribution acting on a rectangle having size $D_V \times D_C$, shown in Fig. 2(b).

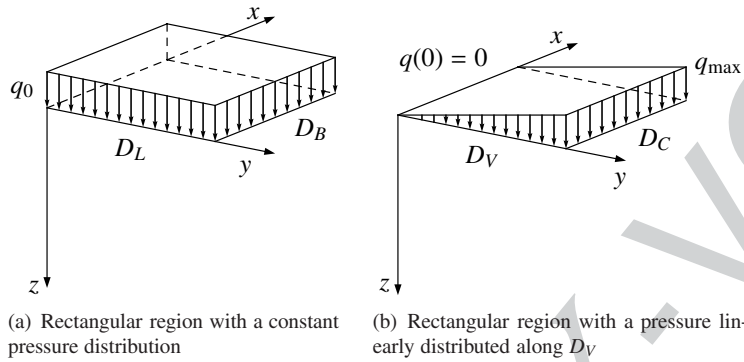


Fig. 2 Elementary load cases for a rectangular loaded region.

The chart plotting the adimensional value σ_z/q_0 for a uniform pressure distribution as a function of different values of the ratio D_B/D_L is reported in Fig. 3(a); analogously the value σ_z/q_{\max} for a linear pressure distribution is plotted in Fig. 3(b) as function of the ratio D_C/D_V . For the reader's convenience, the data plotted in Figs. 3(a) and 3(b) are also reported in Tables 1 and 2, respectively.

Clearly, the solution for any linear load distribution over a rectangular domain, see e.g. Fig. 4(a), can be obtained by super-imposing the effects of three elementary load cases as in Figs. 4(b)–4(d). In particular the case of Fig. 4(b) is evaluated by using the chart in Fig. 3(a) by setting $q_0 = q_a$. Similarly the chart in Fig. 3(b) can be used twice, by properly selecting the values q_{\max} , D_V , and D_C , for addressing the pressure distributions of Fig. 4(c) and Fig. 4(d).

Data reported in Fig. 3 can also be used when one needs to evaluate the stress at a point Q which is not located under a corner of the rectangular region. In this case, two different situations may occur: P inside the loaded rectangle, see Fig. 5(a), or P outside the rectangle, see Fig. 5(b).

In order to evaluate the vertical stress at the point Q in Fig. 5(a) the approach illustrated in Fig. 4 can be applied to the four rectangles $PFCG$, $PGDH$, $PHAE$, and $PEBF$ in Fig. 6 and the contribution of each rectangle shall then be summed up to obtain the final result:

$$\sigma_z^{ABCD} = \sigma_z^{PFCG} + \sigma_z^{PGDH} + \sigma_z^{PHAE} + \sigma_z^{PEBF}. \quad (78)$$

In particular the four addends on the right-hand side can be evaluated by using the charts of Fig. 3 together with the data of Table 3 in which it has to be set:

$$q_p = q_a + \frac{q_b - q_a}{L_1 + L_2} L_1 + \frac{q_d - q_a}{B_1 + B_2} B_1. \quad (79)$$

A similar method applies to the case of Fig. 5(b). The actual load, distributed over the rectangle $ABCD$ and defined by the pressure values q_a , q_b , q_c , and q_d , is supposed to be extended to the rectangle $AEPH$ in Fig. 7 so as to exploit the solution plotted in Fig. 4.

Table 1 Stress ratios σ_z/q_0 due to a uniform pressure distribution over the rectangle of Fig. 2(a).

z/D_L	D_B/D_L						
	0.1	0.2	0.5	1	2	5	10
0	0.25	0.25	0.25	0.25	0.25	0.25	0.25
0.25	1.1527E-1	1.8469E-1	2.3912E-1	2.4729E-1	2.4836E-1	2.4846E-1	2.4846E-1
0.5	6.1001E-2	1.1342E-1	1.9994E-1	2.3247E-1	2.3912E-1	2.3985E-1	2.3987E-1
0.75	3.9578E-2	7.6414E-2	1.5611E-1	2.0598E-1	2.2172E-1	2.2390E-1	2.2397E-1
1	2.7935E-2	5.4714E-2	1.2018E-1	1.7522E-1	1.9994E-1	2.0440E-1	2.0457E-1
1.5	1.5793E-2	3.1273E-2	7.3216E-2	1.2104E-1	1.5611E-1	1.6649E-1	1.6700E-1
2	9.9453E-3	1.9775E-2	4.7533E-2	8.4027E-2	1.2018E-1	1.3628E-1	1.3736E-1
3	4.8608E-3	9.6956E-3	2.3796E-2	4.4734E-2	7.3216E-2	9.5926E-2	9.8677E-2
4	2.8368E-3	5.6650E-3	1.4013E-2	2.7021E-2	4.7533E-2	7.1197E-2	7.5845E-2
6	1.2962E-3	2.5905E-3	6.4454E-3	1.2676E-2	2.3796E-2	4.3111E-2	5.0560E-2
8	7.3639E-4	1.4722E-3	3.6705E-3	7.2709E-3	1.4013E-2	2.8334E-2	3.6733E-2
10	4.7349E-4	9.4674E-4	2.3627E-3	4.6963E-3	9.1685E-3	1.9775E-2	2.7935E-2
12	3.2965E-4	6.5918E-4	1.6460E-3	3.2778E-3	6.4454E-3	1.4469E-2	2.1881E-2
15	2.1142E-4	4.2279E-4	1.0561E-3	2.1065E-3	4.1671E-3	9.6956E-3	1.5793E-2
18	1.4698E-4	2.9395E-4	7.3447E-4	1.4661E-3	2.9099E-3	6.9126E-3	1.1841E-2
20	1.1912E-4	2.3822E-4	5.9528E-4	1.1887E-3	2.3627E-3	5.6650E-3	9.9453E-3

Table 2 Stress ratios σ_z/q_{\max} due to a linear pressure distribution over the rectangle of Fig. 2(b).

z/D_V	D_C/D_V						
	0.1	0.2	0.5	1	2	5	10
0	0.0	0.0	0.0	0.0	0.0	0.0	0.0
0.25	1.4551E-2	2.4410E-2	3.4567E-2	3.6971E-2	3.7401E-2	3.7447E-2	3.7448E-2
0.5	1.4189E-2	2.6752E-2	4.9772E-2	6.0566E-2	6.3309E-2	6.3651E-2	6.3661E-2
0.75	1.2349E-2	2.3967E-2	5.0253E-2	6.8649E-2	7.5326E-2	7.6357E-2	7.6392E-2
1	1.0224E-2	2.0070E-2	4.4650E-2	6.6595E-2	7.7378E-2	7.9491E-2	7.9572E-2
1.5	6.7264E-3	1.3328E-2	3.1322E-2	5.2254E-2	6.8222E-2	7.3185E-2	7.3437E-2
2	4.5188E-3	8.9872E-3	2.1633E-2	3.8393E-2	5.5314E-2	6.3083E-2	6.3618E-2
3	2.3246E-3	4.6369E-3	1.1384E-2	2.1423E-2	3.5156E-2	4.6244E-2	4.7608E-2
4	1.3828E-3	2.7613E-3	6.8312E-3	1.3177E-2	2.3205E-2	3.4846E-2	3.7152E-2
6	6.4070E-4	1.2805E-3	3.1861E-3	6.2662E-3	1.1767E-2	2.1339E-2	2.5044E-2
8	3.6582E-4	7.3135E-4	1.8234E-3	3.6121E-3	6.9622E-3	1.4083E-2	1.8267E-2
10	2.3576E-4	4.7141E-4	1.1765E-3	2.3385E-3	4.5655E-3	9.8492E-3	1.3918E-2
12	1.6435E-4	3.2864E-4	8.2061E-4	1.6342E-3	3.2135E-3	7.2147E-3	1.0913E-2
15	1.0551E-4	2.1100E-4	5.2710E-4	1.0513E-3	2.0797E-3	4.8391E-3	7.8831E-3
18	7.3398E-5	1.4678E-4	3.6676E-4	7.3212E-4	1.4531E-3	3.4520E-3	5.9135E-3
20	5.9496E-5	1.1898E-4	2.9733E-4	5.9374E-4	1.1801E-3	2.8296E-3	4.9678E-3

Accordingly, the contribution of the rectangles *PHDF* and *PGBE* need to be subtracted from the value of the stress relevant to the rectangle *PHAE*. Finally, since the area of the rectangle *PGCF* is included both into the rectangles *PHDF* and *PGBE*, its contribution has to be further summed to the result:

$$\sigma_z^{ABCD} = \sigma_z^{PHAE} - \sigma_z^{PHDF} - \sigma_z^{PGBE} + \sigma_z^{PGCF}. \quad (80)$$

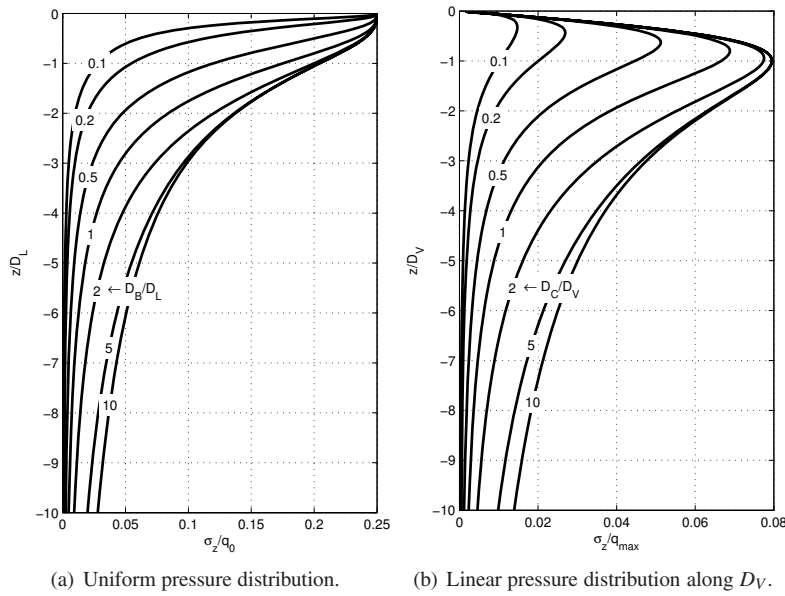


Fig. 3 Stress ratios for the rectangular loaded region of Fig. 2.

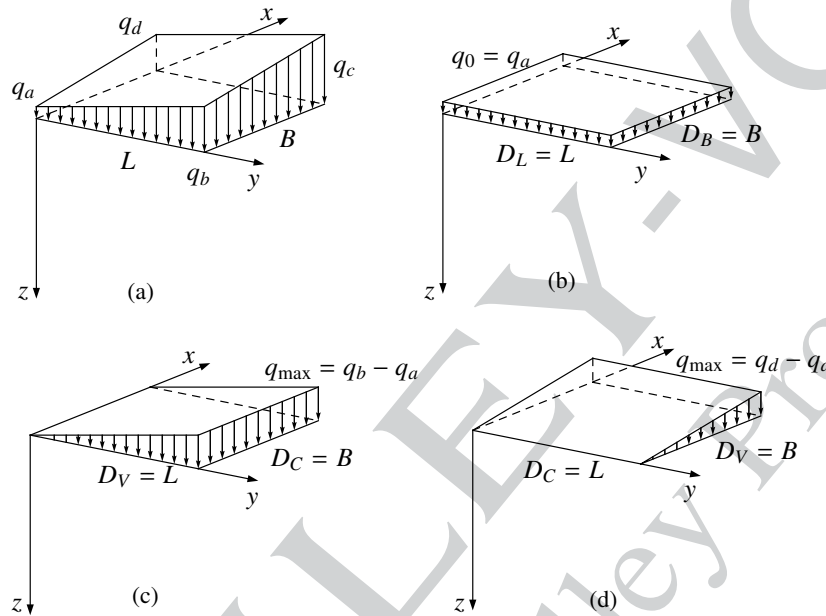


Fig. 4 Rectangular region with an arbitrary bi-linear load distribution and its decomposition into simple load cases.

The four addends on the right-hand side can be evaluated by using the charts of Fig. 3 with the data of Table 4 where:

$$q_p = q_a + \frac{q_b - q_a}{L}(L + L_3) + \frac{q_d - q_a}{B}(B + B_3). \quad (81)$$

In conclusion the charts of Fig. 3 allow one to evaluate by hand the vertical stress due to any rectangular distribution of pressures, a very common situation in civil engineering.

7.2 Circular domain subject to a linear pressure distribution

Let us now address the case of a linear pressure distribution acting on a circular domain of radius R and suppose that one wants to evaluate the vertical stress at a distance L from the center of the loaded region. According to formula (3) σ_z can be evaluated by superimposing two elementary cases.

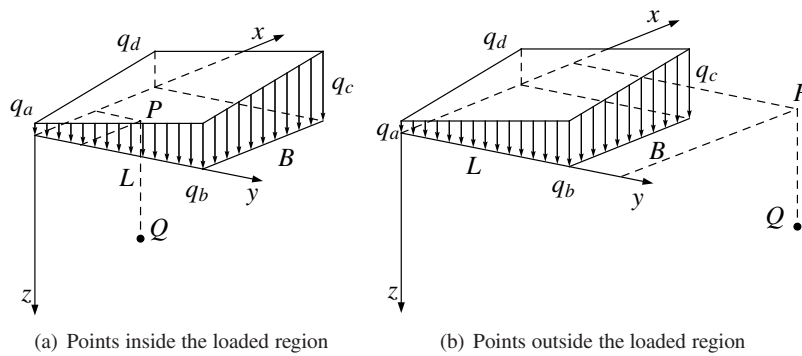


Fig. 5 Evaluation of the stress at points arbitrarily placed with respect to the loaded region.

Table 3 Data for the evaluation of σ_z for the load distribution in of Fig. 6.

	Fig. 3(a)	Fig. 3(b)	Fig. 3(b)
σ_z^{PFCG}	$q_0 = q_p$ $D_B = B_2$ $D_L = L_2$	$q_{\max} = \frac{q_b - q_a}{L_1 + L_2} L_2$ $D_C = B_2$ $D_V = L_2$	$q_{\max} = \frac{q_d - q_a}{B_1 + B_2} B_2$ $D_C = L_2$ $D_V = B_2$
σ_z^{PGDH}	$q_0 = q_p$ $D_B = L_1$ $D_L = B_2$	$q_{\max} = \frac{q_d - q_a}{B_1 + B_2} B_2$ $D_C = L_1$ $D_V = B_2$	$q_{\max} = -\frac{q_b - q_a}{L_1 + L_2} L_1$ $D_C = B_2$ $D_V = L_1$
σ_z^{PHAE}	$q_0 = q_p$ $D_B = B_1$ $D_L = L_1$	$q_{\max} = -\frac{q_b - q_a}{L_1 + L_2} L_1$ $D_C = B_1$ $D_V = L_1$	$q_{\max} = -\frac{q_d - q_a}{B_1 + B_2} B_1$ $D_C = L_1$ $D_V = B_1$
σ_z^{PEBF}	$q_0 = q_p$ $D_B = L_2$ $D_L = B_1$	$q_{\max} = -\frac{q_d - q_a}{B_1 + B_2} B_1$ $D_C = L_2$ $D_V = B_1$	$q_{\max} = \frac{q_b - q_a}{L_1 + L_2} L_2$ $D_C = B_1$ $D_V = L_2$

Table 4 Data for the evaluation of σ_z for the load distribution of Fig. 7.

	Fig. 3(a)	Fig. 3(b)	Fig. 3(b)
σ_z^{PHAE}	$q_0 = q_p$ $D_B = B_3 + B$ $D_L = L_3 + L$	$q_{\max} = -\frac{q_b - q_a}{L} (L_3 + L)$ $D_C = B_3 + B$ $D_V = L_3 + L$	$q_{\max} = -\frac{q_d - q_a}{B} (B_3 + B)$ $D_C = L_3 + L$ $D_V = B_3 + B$
σ_z^{PHDF}	$q_0 = q_p$ $D_B = B_3$ $D_L = L_3 + L$	$q_{\max} = -\frac{q_b - q_a}{L} (L_3 + L)$ $D_C = B_3$ $D_V = L_3 + L$	$q_{\max} = -\frac{q_d - q_a}{B} B_3$ $D_C = L_3 + L$ $D_V = B_3$
σ_z^{PGBE}	$q_0 = q_p$ $D_B = B_3 + B$ $D_L = L_3$	$q_{\max} = -\frac{q_b - q_a}{L} L_3$ $D_C = B_3 + B$ $D_V = L_3$	$q_{\max} = -\frac{q_d - q_a}{B} (B + B_3)$ $D_C = L_3$ $D_V = B_3 + B$
σ_z^{PGCF}	$q_0 = q_p$ $D_B = B_3$ $D_L = L_3$	$q_{\max} = -\frac{q_b - q_a}{L} L_3$ $D_C = B_3$ $D_V = L_3$	$q_{\max} = -\frac{q_d - q_a}{B} B_3$ $D_C = L_3$ $D_V = B_3$

The first one is a constant pressure distribution of value q_0 , see Fig. 8(a). The relevant stress ratios σ_z/q_0 , evaluated for several values of L/R and z/R , are reported in Table 5 and plotted in Fig. 9(a).

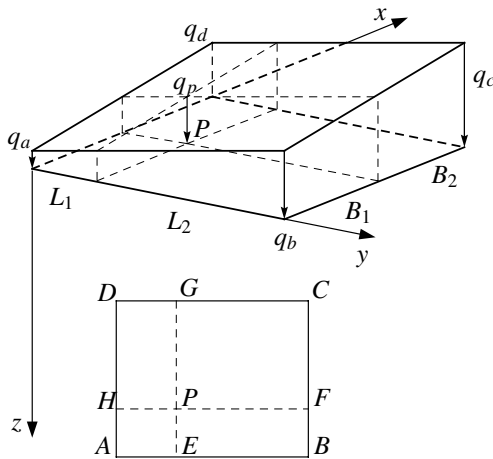


Fig. 6 Composition of loaded regions to address the case of Fig. 5(a).

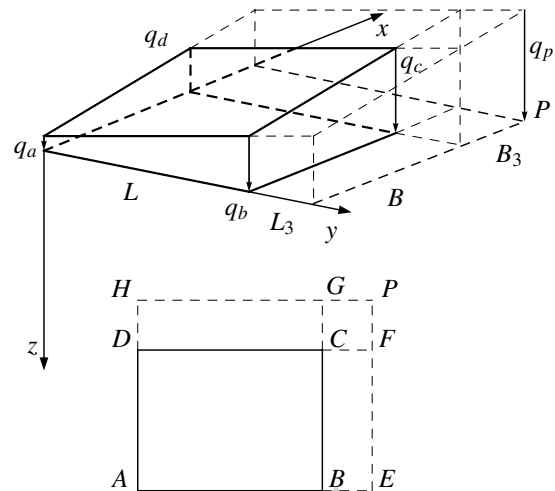
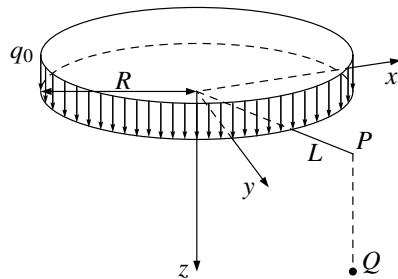
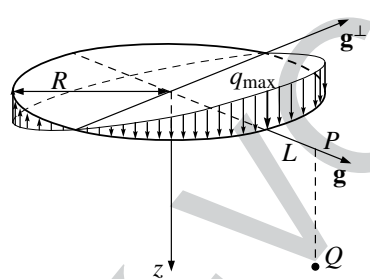


Fig. 7 Composition of loaded regions to address the case of Fig. 5(b).



(a) Circular region with a constant pressure distribution



(b) Circular region with a linear pressure distribution

Fig. 8 Elementary load cases for a circular loaded region.

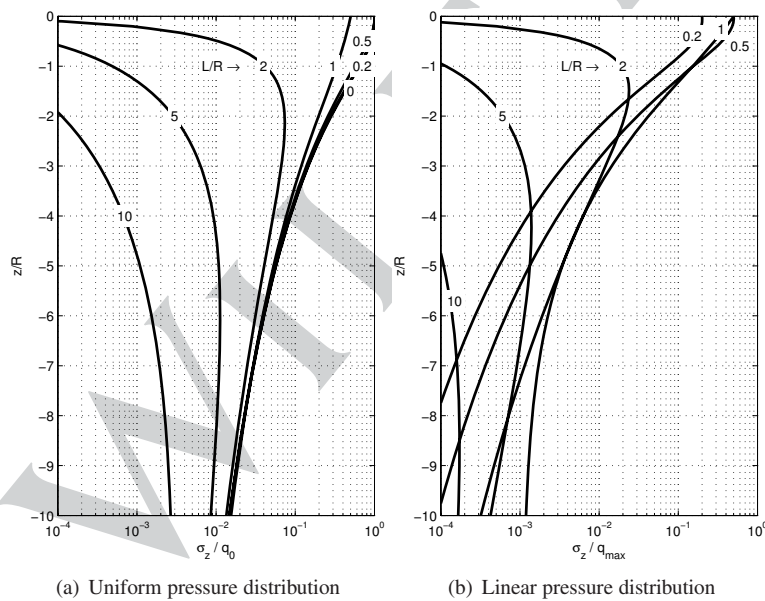


Fig. 9 Stress ratios for the circular loaded region of Fig. 8.

The second elementary case, addressing a linear pressure distribution, is illustrated in Fig. 8(b). In this respect we remark that, \mathbf{g}^\perp and the z axis define an antisymmetric plane for such a pressure distribution; hence the effects of this load case have

Table 5 Stress ratios σ_z/q_0 due to a uniform pressure distribution over the circle of Fig. 8(a).

z/R	L/R						
	0	0.2	0.5	1	2	5	10
0	1.0	1.0	1.0	0.5	0.0	0.0	0.0
0.25	9.8573E-1	9.8369E-1	9.6583E-1	4.6062E-1	1.6463E-3	8.4597E-6	2.4146E-7
0.5	9.1056E-1	9.0158E-1	8.3956E-1	4.1849E-1	1.0472E-2	6.6272E-5	1.9224E-6
0.75	7.8400E-1	7.7047E-1	6.9155E-1	3.7546E-1	2.5567E-2	2.1607E-4	6.4363E-6
1	6.4644E-1	6.3313E-1	5.6222E-1	3.3325E-1	4.1809E-2	4.8842E-4	1.5087E-5
1.5	4.2396E-1	4.1584E-1	3.7504E-1	2.5725E-1	6.5018E-2	1.4470E-3	4.9331E-5
2	2.8446E-1	2.8020E-1	2.5889E-1	1.9701E-1	7.3334E-2	2.8916E-3	1.1194E-4
3	1.4618E-1	1.4491E-1	1.3844E-1	1.1912E-1	6.6630E-2	6.3640E-3	3.3491E-4
4	8.6924E-2	8.6452E-2	8.4027E-2	7.7077E-2	5.2605E-2	9.2280E-3	6.7698E-4
6	4.0265E-2	4.0160E-2	3.9615E-2	3.8763E-2	3.1374E-2	1.1245E-2	1.5239E-3
8	2.2988E-2	2.2953E-2	2.2772E-2	2.3156E-2	1.9850E-2	1.0274E-2	2.2490E-3
10	1.4815E-2	1.4800E-2	1.4724E-2	1.5472E-2	1.3459E-2	8.5604E-3	2.6640E-3
12	1.0327E-2	1.0320E-2	1.0283E-2	1.1166E-2	9.6531E-3	6.9560E-3	2.7933E-3
15	6.6298E-3	6.6269E-3	6.6116E-3	7.5711E-3	6.3468E-3	5.1062E-3	2.6594E-3
18	4.6118E-3	4.6104E-3	4.6030E-3	5.5904E-3	4.4734E-3	3.8342E-3	2.3619E-3
20	3.7383E-3	3.7374E-3	3.7325E-3	4.7289E-3	3.6469E-3	3.2151E-3	2.1450E-3

to be antisymmetric as well. Accordingly, the vertical stress σ_z is zero at every point lying on the vertical plane containing \mathbf{g}^\perp . Conversely, if Q lies in the plane $\mathbf{g} - z$ the stress σ_z at Q is different from zero and the stress ratios σ_z/q_{\max} are reported in Table 6 and Fig. 9(b) for several values of the ratios L/R and z/R .

Table 6 Stress ratios σ_z/q_{\max} due to a linear pressure distribution over the circle of Fig. 8(b).

z/R	L/R						
	0	0.2	0.5	1	2	5	10
0	0.0	0.2	0.5	1.0	0.0	0.0	0.0
0.25	0.0	1.9245E-1	4.6775E-1	3.8591E-1	9.5798E-4	2.0920E-6	3.0101E-8
0.5	0.0	1.5816E-1	3.5545E-1	2.8745E-1	5.7779E-3	1.6263E-5	2.3920E-7
0.75	0.0	1.1233E-1	2.3961E-1	2.0967E-1	1.3020E-2	5.2359E-5	7.9833E-7
1	0.0	7.3945E-2	1.5557E-1	1.5129E-1	1.9285E-2	1.1632E-4	1.8632E-6
1.5	0.0	3.0750E-2	6.6303E-2	7.8665E-2	2.3865E-2	3.2844E-4	6.0173E-6
2	0.0	1.3662E-2	3.0522E-2	4.2255E-2	2.1130E-2	6.1609E-4	1.3423E-5
3	0.0	3.5780E-3	8.3870E-3	1.4426E-2	1.2044E-2	1.1547E-3	3.8308E-5
4	0.0	1.2621E-3	3.0315E-3	6.2850E-3	6.2873E-3	1.3879E-3	7.2743E-5
6	0.0	2.7045E-4	6.6328E-4	2.2534E-3	1.9131E-3	1.1386E-3	1.3961E-4
8	0.0	8.8113E-5	2.1786E-4	1.4326E-3	7.1887E-4	7.1473E-4	1.7084E-4
10	0.0	3.6589E-5	9.0818E-5	1.1908E-3	3.2029E-4	4.2493E-4	1.6596E-4
12	0.0	1.7778E-5	4.4221E-5	1.1006E-3	1.6190E-4	2.5580E-4	1.4267E-4
15	0.0	7.3265E-6	1.8257E-5	1.0498E-3	6.8966E-5	1.2715E-4	1.0203E-4
18	0.0	3.5451E-6	8.8428E-6	1.0313E-3	3.3985E-5	6.8464E-5	6.9488E-5
20	0.0	2.3293E-6	5.8126E-6	1.0253E-3	2.2508E-5	4.7166E-5	5.3527E-5

The charts of Fig. 9 have been obtained by modeling the circular region by means of a regular polygon of 1000 sides and adopting the formulas described in the previous sections. Such charts can be used for the hand evaluation of the vertical stress induced by arbitrary linear pressure distributions over circular domains, see Fig. 10.

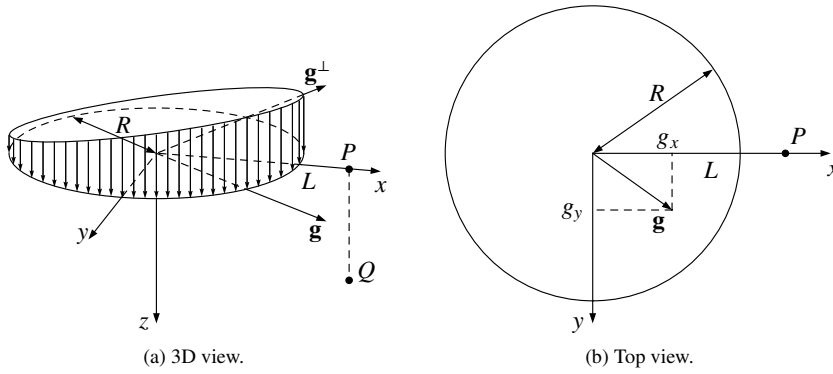


Fig. 10 General case of a circular loaded region.

Suppose, for instance, that a linear pressure distribution $q(\rho) = q_0 + \mathbf{g} \cdot \boldsymbol{\rho}$ is assigned in a reference frame whose axis x connects the center of loaded region with the point P along the vertical at which the vertical stress has to be computed. Such a distribution can be seen as the superposition of three elementary load cases: a constant pressure distribution of value q_0 and two linear pressure distributions with a gradient g_x and g_y , where g_x and g_y are the components of \mathbf{g} .

Comparing the y axis with \mathbf{g}^\perp in Fig. 8(b) one recognizes that the linear pressure distribution having gradient g_y does not induce any σ_z at Q . Hence the vertical stress at Q can be computed by using the charts of Fig. 9, by setting $q_{\max} = g_x R$.

7.3 Wall foundation

Let us consider the finite element model of a wall and its footing depicted in Fig. 11(a). The walls and the footing have thickness equal to 20 cm, Young modulus $E_s = 35$ kPa, and Poisson ratio $\nu_s = 0.2$. Walls have been modeled by means of shell elements and are loaded by nodal forces, expressed in kN in the plot of Fig. 11(a). The footing has been modeled by plate elements on Winkler soil whose stiffness has been assumed equal to $k_w = 20$ N/cm³.

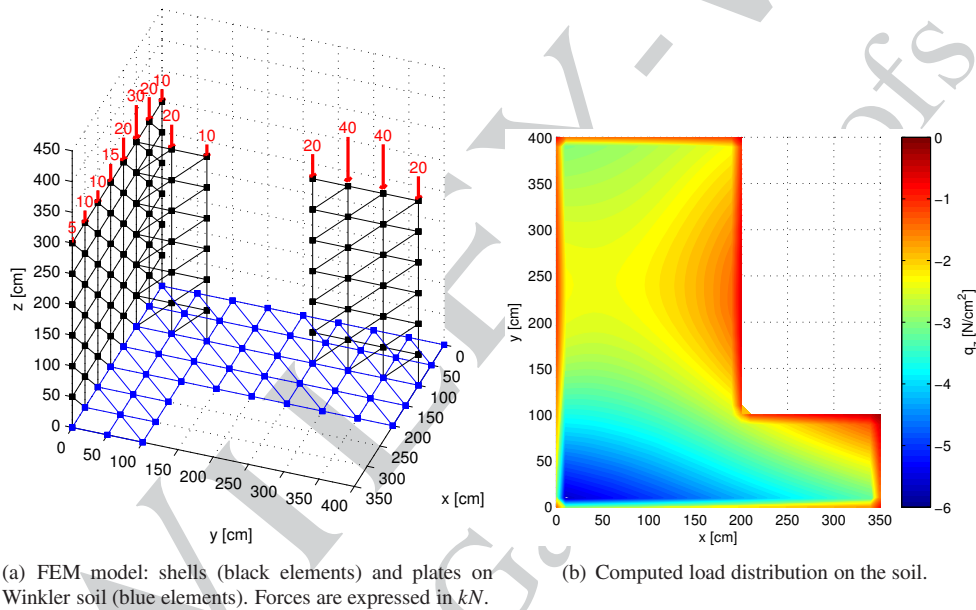


Fig. 11 L-shaped footing.

Since the transverse (out-of-plane) displacements of triangular plate elements are represented by third-order polynomials and a constant Winkler coefficient has been assumed for the soil, the load applied to the soil by each element is actually represented by formula (3). The load distribution is contour-plotted in Fig. 11(b) and is used as input for evaluating the vertical stresses induced in the half-space by means of the proposed formulas.

The results have been obtained at a grid of approximatively 1500 points of the half-space whose coordinates uniformly span the intervals:

$$x \in [-100, 500], \quad y \in [-100, 500], \quad z \in [-400, 0] \quad (82)$$

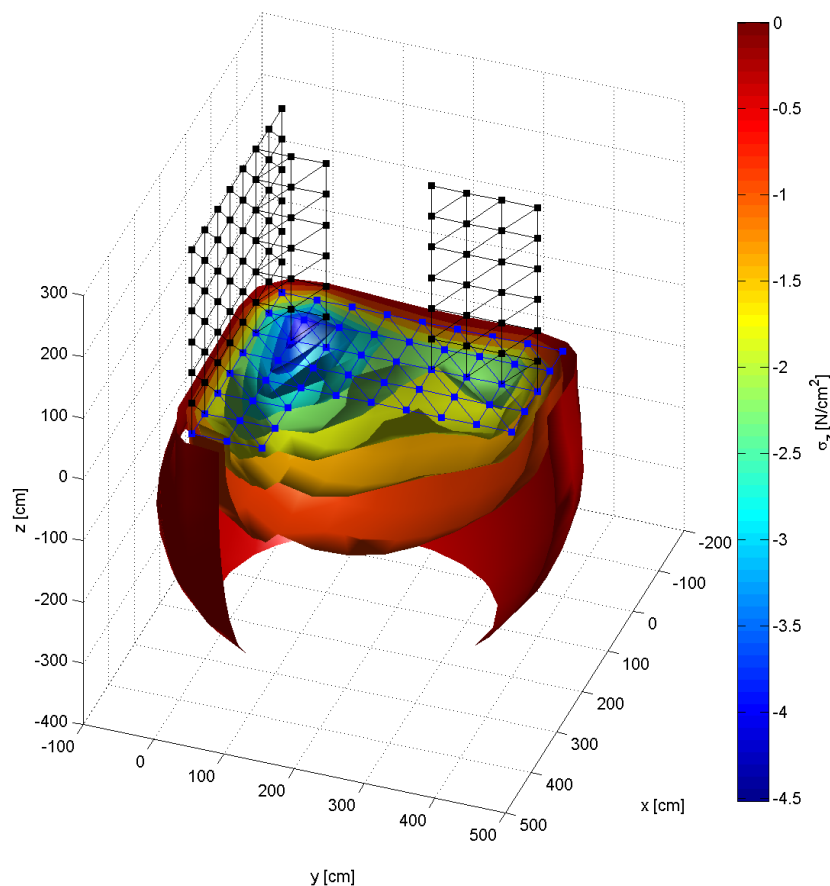


Fig. 12 L-shaped footing: analytical vertical stress distribution within the half-space.

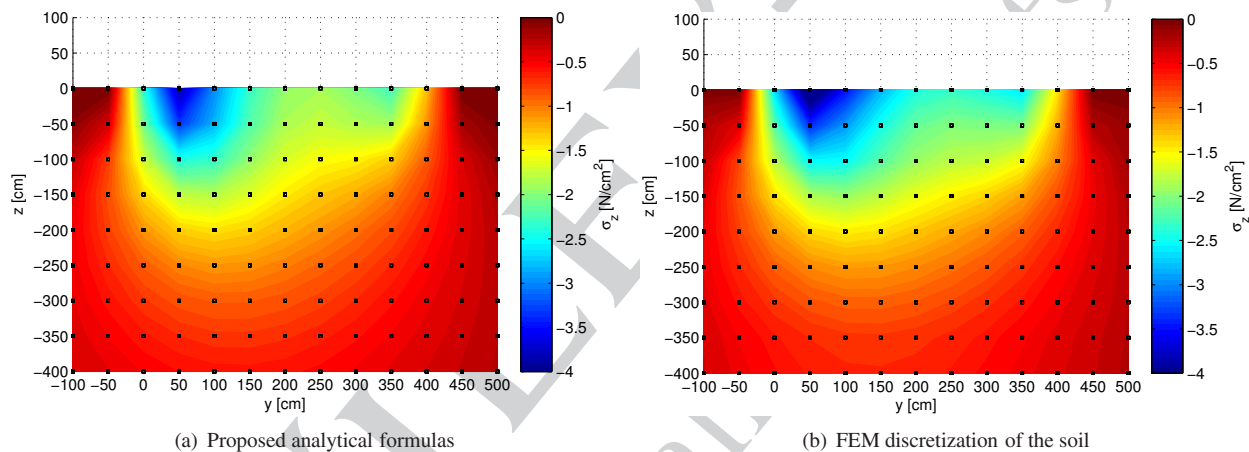


Fig. 13 L-shaped footing: Analytical vs. FEM evaluation of the vertical stresses at the points of the plane $x = 100$ in Fig. 12.

where lengths are expressed in centimeters. The vertical stress σ_z has been represented by means of isostress surfaces reported in the 3D view of Fig. 12.

The same problem has been solved by adopting a finite element model of the soil in which a mesh of 3600 solid elements of size $50 \times 50 \times 50$ cm and 4400 nodes has been adopted. The load distribution of Fig. 11(b) has been applied to the top surface of the model and the vertical stresses have been computed at the Gauss points of each element.

In order to perform a comparison between the results obtained by the proposed formulas and the 3D FEM model, we report in Fig. 13 the contour plot of the vertical stresses computed at the points of the plane $x = 100$ in Fig. 12. Although the results of both analyses are almost coincident, the superiority of the proposed formulas stems from the fact that they allow for an analytical evaluation of the vertical stress at any point of the half space without the need of any soil discretization, what necessarily introduces modeling approximations whose order of magnitude is function of the mesh size.

8 Conclusions

By exploiting concepts and results of potential theory it has been illustrated a general methodology to evaluate analytically the vertical stress within a homogeneous isotropic elastic half-space due to pressures distributed with a nonlinear law over polygonal domains of arbitrary shape. Charts have been provided as design aids in order to allow one for the evaluation of vertical stress by hand calculations in the case of rectangles or circles loaded by a linear pressure distribution.

References

- [1] H. M. Algin, Stresses from linearly distributed pressures over rectangular areas, *Int. J. Numer. Anal. Meth. Geomech.* **24**, 681–692 (2000).
- [2] H. M. Algin, Vertical stress formula for pressure over rectangular areas, *Geotechnique* **51**(8), 719–722 (2001).
- [3] R. J. Blakely, *Potential Theory in Gravity and Magnetic Applications* (Cambridge University Press, Cambridge, 1996).
- [4] J. Boussinesq, *Applications des Potentials a l'Etude de l'Equilibre et Mouvement des Solides Elastiques* (Gauthier-Villard, Paris, 1885).
- [5] R. M. Bowen and C. C. Wang, *Introduction to Vectors and Tensors, Vol. 2: Vector and Tensor Analysis*. Available electronically from <http://hdl.handle.net/1969.1/3609>. Date of access (Dec. 2012).
- [6] J. E. Bowles, *Foundation Analysis and Design* (McGraw-Hill, New York, 1996), pp. 285–300.
- [7] J. A. Charles, The depth of influence of loaded areas, *Geotechnique* **46**, 51–61 (1996).
- [8] D. Dong, P. Fang, Y. Bock, M. Cheng, and S. Miyazaki, Anatomy of apparent seasonal variations from GPS-derived site position time series, *J. Geophys. Res.* **107**, ETG, 9.1–9.18 (2002).
- [9] M. G. D'Urso and P. Russo, A new algorithm for point-in polygon test, *Surv. Rev.* **36**, 284 (2002).
- [10] M. G. D'Urso and F. Marmo, Vertical Stresses Due to Linearly Distributed Pressures Over Polygonal Domains, *Proceedings ComGeo I, First International Symposium on Computational Geomechanics*, 29 April, 1 May 2009, Juan les Pins, France (IC2E International Centre for Computational Engineering, Rhodes, Greece 2009).
- [11] M. G. D'Urso, New Expressions of the Gravitational Potential and its Derivates for the Prism, *VII Hotine-Marussi International Symposium on Mathematical Geodesy*, edited by N. Neeuw, P. Novák, M. Crespi, and F. Sansò (Springer-Verlag, Berlin, Heidelberg, 2012).
- [12] M. G. D'Urso, On the evaluation of the gravity effects of polyhedral bodies and a consistent treatment of related singularities, *J. Geodesy* **87**, 239–252 (2013).
- [13] M. G. D'Urso, Analytical computation of gravity effects for polyhedral bodies, submitted to *J. Geodesy* (2013).
- [14] M. G. D'Urso, A Remark on the Computation of the Gravitational Potential of Masses with Linearly Varying Density, edited by M. Crespi and F. Sansò, *Proceedings of the VIII Hotine Marussi Symposium*, June 17–21, (Int. Assoc. Geodesy, Rome, Italy, 2013).
- [15] M. G. D'Urso and F. Marmo, On a generalized Love's problem. Accepted for publication in *Comput. Geosci.* (2013).
- [16] R. E. Gibson, Some results concerning displacements and stresses in a non-homogeneous elastic half-space, *Geotechnique* **17**, 58–67 (1967).
- [17] R. E. Gibson, The analytical methods in soil mechanics, *Geotechnique* **24**, 115–140 (1974).
- [18] K. L. Johnson, *Contact Mechanics* (Cambridge University Press, New York, 1985).
- [19] H. Lamb, On Boussinesq's problem, *Proc. Lond. Math. Soc.* **34**, 276–284 (1902).
- [20] A. E. H. Love, The stress produced in a semi-infinite solid by pressure on part of the boundary, *Philos. Trans. R. Soc. Lond. A* **667**, 377–420 (1929).
- [21] S. Mangiarotti, A. Cazenave, L. Soudarin, and J. Cretaux, Annual vertical crustal motions predicted from surface mass redistribution and observed by space geodesy, *J. Geophys. Res.* **106**, 4277–4291 (2001).
- [22] N. M. Newmark, *Simplified Computation of Vertical Pressures in Elastic Foundations*, Circular No. 24, (University of Illinois Engineering Experiment Station, Illinois, 1935), pp. 19.
- [23] H. G. Poulos and E. H. Davis, *Elastic Solutions for Soil and Rock Mechanics* (Wiley, New York, 1974).
- [24] A. P. S. Selvadurai, The analytical method in geomechanics, *Appl. Mech. Rev.* **60**, 87–106 (2007).
- [25] M. Skrinar, Generalisation of Boussinesq's equation over triangularly shaped bases, *Z. Angew. Math. Mech.* **80**(2), 553–554 (2000).
- [26] W. Steinbrenner, A rational method for the determination of the vertical normal stresses under foundations, *Harvard Proc. Int. Conf. on Soil Mech. Found. Eng.* **2**, 142–143 (1936).
- [27] K. T. Tang, *Mathematical methods for engineers and scientists* (Springer, Berlin, Heidelberg, New York, 2006).
- [28] S. Timoshenko and J. N. Goodier, *Theory of Elasticity* (McGraw-Hill, New York, 1951).
- [29] D. M. Vitone and A. J. Valsangkar, Stresses from loads over rectangular areas, *J. Geotech. Eng. Div. ASCE* **112**(10), 961–964 (1986).
- [30] C. Vrettos, The Boussinesq problem for soils with bounded non-homogeneity, *Int. J. Numer. Anal. Meth. Geomech.* **22**, 655–669 (1998).
- [31] C. D. Wang, C. S. Tzeng, E. Pan, and J. J. Liao, Displacements and stresses due to a vertical point load in an inhomogeneous transversely isotropic half-space, *Int. J. Rock Mech. Mining Sci.* **40**, 667–685 (2003).